



Mixed convection nonaxisymmetric Homann stagnation-point flow under the influence of magnetic field

Chhatu Manuel Mardi¹ , Tapas Ray Mahapatra² 

Department of Mathematics, Visva-Bharati (A Central University),
Santiniketan – 731 235, West-Bengal, India
papaimardi96@gmail.com; trmahapatra@yahoo.com

Received: July 6, 2023 / **Revised:** October 27, 2024 / **Published online:** December 1, 2024

Abstract. In the present study, we have investigated the steady mixed convection nonaxisymmetric Homann stagnation-point flow in the presence of a magnetic field over a vertical flat wall immersed in a viscous and incompressible fluid. The magnetic field is applied in the normal direction to the plate. The governing equations are reduced to a system of nonlinear ordinary differential equations with suitable boundary conditions by applying similarity transformations to the equations and the boundary conditions. Using an efficient shooting method, the transformed equations are numerically solved. The solution involves the dimensionless governing parameters: γ representing the shear-to-strain-rate ratio, a mixed convection parameter λ , a magnetic field parameter M , and Prandtl number Pr . An important observation is that dual solutions exist for a certain range of mixed convection parameter λ . It is noticed that critical values λ_c of λ are found in opposing flow, which produce two solution branches by making saddle-node bifurcation at $\lambda = \lambda_c$. Numerical results are obtained for representative values of γ , λ , and M and are explored in depth. Through the use of graphs, the properties of the flow and temperature profiles for various values of the governing parameters γ , λ , and M are examined. Also, we examined how the solution varied with λ for representative values of M (magnetic field parameter). A parametric analysis is conducted to investigate how different governing parameters affect the characteristics of fluid flow and temperature. Also, we derive asymptotic results for large λ .

Keywords: asymptotic solutions, stagnation-point flow, dual solutions, mixed convection.

1 Introduction

Mixed convection flows arise when the buoyancy forces resulting from temperature differences within the flow become comparable to the pressure gradient forces arising from the forced flow. As a consequence, both the flow and thermal fields are significantly affected by the buoyancy forces. Mixed convection flows (combined forced and free

¹The author was supported by the Council of Scientific and Industrial Research (CSIR), New Delhi, File No. 09/202(0104)/2019-EMR-I.

²Corresponding author.

convection boundary layer flows) have been the subject of great attention to scientists from both practical and theoretical points of view. The significance of this is due to the widespread occurrence of convective flows in numerous engineering and geophysical domains, including geothermal energy extraction, nuclear waste disposal, groundwater movement, thermal insulation, solid-matrix heat-exchangers, drying porous solids oil and gas production, and many others. Mixed convection heat transfer is induced by the interaction between internally generated buoyancy forces and an imposed flow, it is also substantial in crystal growth, solar collectors, nuclear reactors, and the cooling of electronic systems. Numerous studies of mixed convection flow of an incompressible and viscous fluid over a vertical surface have already been carried out. The temperature and velocity fields have been solved analytically and numerically for temperatures. In a review study, Chen [3] and the books by Gebhart et al. [6], Schlichting and Gersten [26], Pop and Ingham [23], and Bejan [2] provided a thorough account of the theoretical work done for both laminar and turbulent mixed convection boundary layer flows for a few different flow geometries before 1987. Finding exact (or numerical) solutions to partial differential equations is the objective in many areas of fluid mechanics and heat transport issues. These equations describe the fundamental physical laws. Solutions derived by employing variable transformations that transform the system of partial differential equations into a system of ordinary differential equations are notable among the solutions. These solutions are typically called similarity solutions; see Hansen [8]. Mahmood and Merkin [18, 19], Merkin and Mahmood [21], and Merkin and Pop [22] have published a series of publications presenting similarity solutions for the problem under consideration for the steady mixed convection boundary-layer flow over an impermeable vertical flat plate and for impermeable vertical cylinders.

In fluid mechanics, the study of stagnation-point flow is extremely influential. Two-dimensional stagnation-point flows arise near a stagnation line resulting from a two-dimensional flow impinging on a curved surface at right angles to it and after that flowing symmetrically about the stagnation line. Stagnation-point flows, referred to as flows about the front of a blunt-nosed body or the stagnation region, occur on bodies moving in a fluid. Stagnation-point flows, which describe the fluid motion at the stagnation region at the front of a blunt-nosed body, exist on all solid bodies moving in a fluid. The pressure, heat transmission, and mass deposition rates are all maximum in the stagnation area. Stagnation-point flow is still a topic of interest for scientists and researchers due to its significance in so many different industrial and scientific applications, such as the polymer industry, extrusion processes, plane counter-jets, and numerous forms of hydrodynamic modelling in engineering applications. In recent times, it has drawn a lot of interest from researchers. Hiemenz [10] was the first researcher who utilized a similarity transform to investigate two-dimensional stagnation-point flows by condensing the partial differential Navier–Stokes equations into a set of nonlinear ordinary differential equations. Later, Eckert [4] and Gorla [7] considered the corresponding forced-convection heat-transfer problem. Three-dimensional stagnation-point flows have been studied by Homann [11] and Smith [27], and the axisymmetric stagnation-point flow on a circular cylinder – by Wang [28]. The steady mixed convection flow near the stagnation region of a vertical flat plate has been studied by Ramachandran et al. [24]. The steady two-dimensional boundary

layer flow in the neighborhood of a stagnation point on an infinite wall was studied by Hiemenz [10] using a similarity transform, which reduces the number of independent variables from two to one. This result has been later extended to the axisymmetric case by Homann [11]. Mahapatra and Gupta [14] reinvestigated the stagnation-point flow problem towards a stretching sheet with different stretching and straining rates. Mahapatra and Sidui [16] performed an analysis of unsteady heat transfer in nonaxisymmetric Homann stagnation-point flows of a viscous fluid over a rigid plate. Later, Mahapatra and Sidui [17] carried out research on the nonaxisymmetric Homann stagnation-point flows of a viscoelastic fluid towards a stationary plate.

Magnetohydrodynamics is based on studying the magnetic properties and behaviour of electrically conducting fluids. MHD technology is based on the fundamental law of electromagnetism. The interaction between the fluid velocity and the applied magnetic field generates the Lorentz forces during the movement of fluid. The Lorentz force creates some resistive force to the motion of the fluid particles, which slows down the fluid velocity. There are numerous uses of the boundary layer flow of an electrically conducting fluid in the presence of a magnetic field in engineering problems, such as MHD generator, plasma studies, nuclear reactors, geothermal energy extraction, and oil exploration. Ariel [1] investigated the effect of an external magnetic field on Hiemenz flow. Mahapatra and Gupta [14] examined boundary-layer and magnetohydrodynamics stagnation-point flow towards a sheet that was stretched.

Eldabe and Ouaf [5] considered the problem of heat and mass transfer in an MHD flow of a micropolar fluid past a stretching surface with Ohmic heating and viscous dissipation effects using the Chebyshev finite difference method. Ishak et al. [12] solved the steady MHD stagnation-point flow problem towards a vertical surface immersed in a micropolar fluid. Weidman [29] generalized Homann's problem by superposing periodic terms onto Homann's outer potential flow. Lok et al. [13] extended the work of Weidman [29] by including heat transfer and the effects of the induced buoyancy.

In the present paper, we aim to investigate the magnetic field effects on mixed convection nonaxisymmetric Homann stagnation-point flow over a vertical flat wall. The self-similar equations are solved numerically using MATHEMATICA 10.0, and the outcomes are explained from a physical perspective. The presentation of the paper is as follows. The formulation of the problem is given in Section 2, where a numerical solution of coupled nonlinear ordinary differential equations is discussed, and asymptotic behaviour is reported. A stability analysis of the dual solutions is performed in Section 3. Numerical solution procedure of the system of ordinary differential equations are discussed in Section 4. Section 5 contains the results and discussions. A concluding remark is given in Section 6.

2 Formulation of the problem

Consider the steady mixed convection nonaxisymmetric Homann stagnation-point flow over a vertical flat rigid wall placed in a viscous and incompressible electrically conducting fluid. A uniform magnetic field of strength B_0 is applied in the positive z -direction,

perpendicular to the plate. It is assumed that the surface temperature of the plate is $T_w(x) = T_\infty + T_0x$, where T_∞ is the constant ambient temperature, and T_0 is a characteristic temperature. This is to note that for a heated surface, $T_0 > 0$, and for a cooled surface, $T_0 < 0$. The heated surface induces an aiding flow, whereas the cooled surface induces an opposing flow. The velocity components of the external flow or potential flow are $U_e(x, y) = (a + b)x$, $V_e(x, y) = (a - b)y$, and $W_e(z) = -2az$. Here the z -axis is measured in the normal direction to the wall, and the x -axis is measured in the vertical direction, a is the strain rate of the stagnation-point flow, b is the shear rate. As the fluid is electrical conducting, so the Lorentz force for induced current is given by $\vec{J} \times \vec{B}$, where $\vec{J} = \sigma(\vec{E} + \vec{q} \times \vec{B})$ is the current density. It is also assumed that the conduction current σE is negligible compared to the convection current $\sigma(\vec{q} \times \vec{B})$, where σ is the electrical conductivity, $\vec{q} = u\hat{i} + v\hat{j} + w\hat{k}$ is the fluid velocity, and $\vec{B} = (0, 0, B_0\hat{k})$ is the magnetic field. The magnetic field is applied along z -axis as $\vec{B} = B_0\hat{k}$, then the Lorentz force takes the form $\vec{J} \times \vec{B} = -\sigma B_0^2(u\hat{i} + v\hat{j})$, which are added to the right-hand side of u -momentum and v -momentum equations.

The governing equations, respectively, of continuity, momentum and energy in Cartesian form are given by

$$\frac{\partial u}{\partial x} + \frac{\partial v}{\partial y} + \frac{\partial w}{\partial z} = 0, \quad (1)$$

$$u \frac{\partial u}{\partial x} + v \frac{\partial u}{\partial y} + w \frac{\partial u}{\partial z} = -\frac{1}{\rho} \frac{\partial p}{\partial x} + g\beta(T - T_\infty) + \nu \left(\frac{\partial^2 u}{\partial x^2} + \frac{\partial^2 u}{\partial y^2} + \frac{\partial^2 u}{\partial z^2} \right) - \frac{\sigma B_0^2 u}{\rho}, \quad (2)$$

$$u \frac{\partial v}{\partial x} + v \frac{\partial v}{\partial y} + w \frac{\partial v}{\partial z} = -\frac{1}{\rho} \frac{\partial p}{\partial y} + \nu \left(\frac{\partial^2 v}{\partial x^2} + \frac{\partial^2 v}{\partial y^2} + \frac{\partial^2 v}{\partial z^2} \right) - \frac{\sigma B_0^2 v}{\rho}, \quad (3)$$

$$u \frac{\partial w}{\partial x} + v \frac{\partial w}{\partial y} + w \frac{\partial w}{\partial z} = -\frac{1}{\rho} \frac{\partial p}{\partial z} + \nu \left(\frac{\partial^2 w}{\partial x^2} + \frac{\partial^2 w}{\partial y^2} + \frac{\partial^2 w}{\partial z^2} \right), \quad (4)$$

$$u \frac{\partial T}{\partial x} + v \frac{\partial T}{\partial y} + w \frac{\partial T}{\partial z} = \alpha \left(\frac{\partial^2 T}{\partial x^2} + \frac{\partial^2 T}{\partial y^2} + \frac{\partial^2 T}{\partial z^2} \right) \quad (5)$$

subject to the boundary conditions

$$u = v = w = 0, \quad T = T_w \quad \text{on } z = 0 \\ u \rightarrow U_e, \quad v \rightarrow V_e, \quad w \rightarrow W_e, \quad T \rightarrow T_\infty, \quad p \rightarrow p_0 \quad \text{as } z \rightarrow \infty, \quad (6)$$

where u , v , and w represent the velocity components along x -, y -, and z -directions, respectively, p is the fluid pressure, g is the acceleration due to gravity, ρ is the constant fluid density, β is the coefficient of thermal expansion, ν is the kinematic viscosity, μ is the dynamic viscosity, α is the thermal diffusivity, p_0 is the constant far field pressure. In the right-hand side of Eqs. (2) and (3), the terms $\sigma B_0^2 u / \rho$ and $\sigma B_0^2 v / \rho$ represent the Lorentz force, which generated from the interaction between the fluid velocity and the magnetic field. Further, we have ignored the induced magnetic field since the magnetic Reynolds number for the flow is taken to be very small.

We introduce now the following similarity variables:

$$\begin{aligned}
 u &= (a + b)xf'(\eta), & v &= (a - b)yg'(\eta), \\
 w &= -\sqrt{\frac{\nu}{a}}[(a + b)f(\eta) + (a - b)g(\eta)], \\
 T - T_\infty &= T_0x\theta(\eta), & \eta &= \sqrt{\frac{a}{\nu}}z.
 \end{aligned}
 \tag{7}$$

Substituting transformation (7) into (2), (3), (5), (6), we obtain the following nonlinear ordinary differential equations:

$$\begin{aligned}
 f'''' + (1 + \gamma)(ff'' + 1 - f'^2) + (1 - \gamma)gf'' + (1 + \gamma)\lambda\theta \\
 + M(1 - f') = 0,
 \end{aligned}
 \tag{8}$$

$$g'''' + (1 - \gamma)(gg'' + 1 - g'^2) + (1 + \gamma)fg'' + M(1 - g') = 0,
 \tag{9}$$

$$\frac{1}{Pr}\theta'' + (1 + \gamma)(f\theta' - f'\theta) + (1 - \gamma)g\theta' = 0
 \tag{10}$$

subject to the boundary conditions

$$\begin{aligned}
 f(0) = f'(0) = 0, & \quad g(0) = g'(0) = 0, & \quad \theta(0) = 1, \\
 f' \rightarrow 1, & \quad g' \rightarrow 1, & \quad \theta \rightarrow 0 \quad \text{as } \eta \rightarrow \infty.
 \end{aligned}
 \tag{11}$$

Here primes denote differentiation with respect to the independent variable η , and

$$Pr = \frac{\nu}{\alpha}, \quad \lambda = \frac{g\beta T_0}{(a + b)^2}, \quad \gamma = \frac{b}{a}, \quad M = \frac{\sigma B_0^2}{\rho a}.$$

The pressure field for the viscous incompressible electrically conductivity fluid flow is

$$\begin{aligned}
 p = p_0 - \left[\rho \left\{ \frac{(a + b)^2 x^2}{2} + \frac{(a - b)^2 y^2}{2} \right\} + \sigma B_0^2 \left\{ \frac{(a + b)x^2}{2} + \frac{(a - b)y^2}{2} \right\} \right. \\
 \left. + \rho\nu a \left\{ \frac{[(1 + \gamma)f + (1 - \gamma)g]^2}{2} + (1 + \gamma)f' + (1 - \gamma)g' \right\} \right].
 \end{aligned}$$

The parameter λ represents the strength of the buoyancy force or mixed convection parameter relative to shear-to-strain-rate. It is positive for aiding flow, negative for opposing flow.

The object of this work is in finding the values to skin friction coefficients $f''(0)$, $g''(0)$ and surface temperature gradient $\theta'(0)$ and how they vary in terms of parameters: shear-to-strain-rate ratio γ , mixed convection parameter λ , and magnetic field parameter M . Also, we study the velocity and temperature profiles for different values of the governing parameters. In our results, the Prandtl number Pr is set to be unity ($Pr = 1$). Using an effective shooting method, these problems are numerically solved.

2.1 Forced convection, $\lambda = 0$

We are interested in finding the solution to the flow problem when γ approaches the singularity “-1”. To consider this, we put $\gamma = -1 + \delta$ and write $f = \delta^{-1}F$, while δ is very small. Now Eqs. (8) and (9) become

$$F''' + FF'' - F'^2 + \delta^2 + (2 - \delta)gF'' + M(\delta - F') = 0, \tag{12}$$

$$g''' + (2 - \delta)(gg'' + 1 - g'^2) + Fg'' + M(1 - g') = 0 \tag{13}$$

subject to the boundary conditions derived from (11)

$$F(0) = F'(0) = 0, \quad g(0) = g'(0) = 0, \quad F' \rightarrow \delta, \quad g' \rightarrow 1 \quad \text{as } \eta \rightarrow \infty. \tag{14}$$

Equations (12) and (13) subject to the boundary conditions (14) suggest looking for an expansion of F and g in powers of δ . The leading order terms F_0 and g_0 satisfy

$$F_0''' + F_0F_0'' - F_0'^2 + 2g_0F_0'' - MF_0' = 0,$$

$$g_0''' + 2(g_0g_0'' + 1 - g_0'^2) + F_0g_0'' + M(1 - g_0') = 0$$

subject to the boundary conditions

$$F_0(0) = F_0'(0) = 0, \quad g_0(0) = g_0'(0) = 0, \quad F_0' \rightarrow 0, \quad g_0' \rightarrow 1 \quad \text{as } \eta \rightarrow \infty.$$

For this problem, a numerical solution gives

$$F_0'' = \begin{cases} -1.78068, & M = 0, \\ -1.81993, & M = 0.2, \\ -1.84724, & M = 0.5, \end{cases} \quad g_0'' = \begin{cases} 1.66588, & M = 0, \\ 1.72428, & M = 0.2, \\ 1.80958, & M = 0.5, \end{cases}$$

so that

$$f''(0) \sim \begin{cases} -1.78068(1 + \gamma)^{-1} + \dots, & M = 0, \\ -1.81993(1 + \gamma)^{-1} + \dots, & M = 0.2, \\ -1.84724(1 + \gamma)^{-1} + \dots, & M = 0.5, \end{cases} \tag{15}$$

$$g''(0) \rightarrow \begin{cases} 1.66588 + \dots, & M = 0, \\ 1.72428 + \dots, & M = 0.2, \\ 1.80958 + \dots, & M = 0.5, \end{cases} \tag{16}$$

as $\gamma \rightarrow -1$.

The wall shear stress vector can be written as

$$\vec{\tau}_w = \mu \left[\frac{\partial u}{\partial z} \hat{i} + \frac{\partial v}{\partial z} \hat{j} \right]_{z=0} = \frac{\mu a^{3/2}}{\nu^{1/2}} [(1 + \gamma)f''(0)x\hat{i} + (1 - \gamma)g''(0)y\hat{j}].$$

From Eqs. (15) and (16) it is evident that wall shear stress increases along the x - and y -direction with the increase in the magnetic field intensity.

2.2 Free convection limit, λ large

Suppose that $\gamma \neq -1$, and to determine a solution valid for $\lambda \gg 1$, we put

$$f = \lambda^{1/4}\phi, \quad g = \lambda^{1/4}h, \quad \xi = \lambda^{1/4}\eta.$$

Equations (8)–(11) then become

$$\begin{aligned} \phi'''' + (1 + \gamma)(\phi\phi'' - \phi'^2) + (1 - \gamma)h\phi'' + (1 + \gamma)\lambda^{-1} \\ + (1 + \gamma)\theta + M(\lambda^{-1} - \lambda^{-1/2}\phi') = 0, \\ h'''' + (1 - \gamma)(hh'' - h'^2) + (1 + \gamma)\phi h'' + (1 - \gamma)\lambda^{-1} \\ + M(\lambda^{-1} - \lambda^{-1/2}h') = 0, \\ \frac{1}{Pr}\theta'' + (1 + \gamma)(\phi\theta' - \phi'\theta) + (1 - \gamma)h\theta' = 0 \end{aligned}$$

subject to the boundary conditions

$$\begin{aligned} \phi(0) = \phi'(0) = h(0) = h'(0) = 0, \quad \theta(0) = 1, \\ \phi' \rightarrow \lambda^{-1/2}, \quad h' \rightarrow \lambda^{-1/2}, \quad \theta \rightarrow 0, \quad \text{as } \xi \rightarrow \infty. \end{aligned} \tag{17}$$

Here prime denotes differentiation with respect to ξ . Since $\lambda^{-1/2}$ presents in the boundary conditions (17), we write the solution as

$$\begin{aligned} \phi = \phi_0 + \lambda^{-1/2}\phi_1 + \dots, \quad h = \lambda^{-1/2}h_0 + \lambda^{-1}h_1 + \dots, \\ \theta = \theta_0 + \lambda^{-1/2}\theta_1 + \dots \end{aligned}$$

and obtain, at zero and first order,

$$\phi_0'''' + (1 + \gamma)(\phi_0\phi_0'' - \phi_0'^2) + (1 + \gamma)\theta_0 = 0, \tag{18}$$

$$\begin{aligned} \phi_1'''' + (1 + \gamma)(\phi_0\phi_1'' + \phi_1\phi_0'' - 2\phi_0'\phi_1') \\ + (1 - \gamma)h_0\phi_0'' + (1 + \gamma)\theta_1 - M\phi_0' = 0, \end{aligned} \tag{19}$$

$$h_0'''' + (1 + \gamma)\phi_0h_0'' = 0, \tag{20}$$

$$\begin{aligned} h_1'''' + (1 - \gamma)(h_0h_0'' - h_0'^2 + 1) + (1 + \gamma)(\phi_0h_1'' + \phi_1h_0'') \\ + M(1 - h_0') = 0, \end{aligned} \tag{21}$$

$$\frac{1}{Pr}\theta_0'' + (1 + \gamma)(\phi_0\theta_0' - \phi_0'\theta_0) = 0, \tag{22}$$

$$\frac{1}{Pr}\theta_1'' + (1 + \gamma)(\phi_0\theta_1' + \phi_1\theta_0' - \phi_0'\theta_1 - \phi_1'\theta_0) + (1 - \gamma)h_0\theta_0' = 0 \tag{23}$$

subject to the boundary conditions

$$\begin{aligned} \phi_0(0) = \phi_0'(0) = h_0(0) = h_0'(0) = 0, \quad \theta_0(0) = 1, \\ \phi_1(0) = \phi_1'(0) = h_1(0) = h_1'(0) = 0, \quad \theta_1(0) = 0, \\ \phi_0' \rightarrow 0, \quad \phi_1' \rightarrow 1, \quad h_0' \rightarrow 1, \quad h_1' \rightarrow 0, \quad \theta_0 \rightarrow 0, \quad \theta_1 \rightarrow 0 \quad \text{as } \xi \rightarrow \infty. \end{aligned} \tag{24}$$

A numerical integration of (18)–(24) gives, for $Pr = 1.0$ and $\gamma = 0.6$, when $M = 0$,

$$\begin{aligned}\phi_0''(0) &= 0.935402, & h_0''(0) &= 0.496728, & \theta_0'(0) &= -0.752735, \\ \phi_1''(0) &= -0.011796, & h_1''(0) &= 0.602175, & \theta_1'(0) &= -0.062065, \\ f''(0) &\sim 0.935402\lambda^{3/4} - 0.011796\lambda^{1/4} + \dots, \\ g''(0) &\sim 0.496728\lambda^{1/4} + 0.602175\lambda^{-1/4} + \dots, \\ \theta'(0) &\sim -0.752735\lambda^{1/4} - 0.062065\lambda^{-1/4} + \dots,\end{aligned}$$

for $Pr = 1$ and $\gamma = 0.6$, when $M = 2.5$,

$$\begin{aligned}\phi_0''(0) &= 0.935402, & h_0''(0) &= 0.496728, & \theta_0'(0) &= -0.752735, \\ \phi_1''(0) &= -0.43393, & h_1''(0) &= 2.59746, & \theta_1'(0) &= 0.160829, \\ f''(0) &\sim 0.935402\lambda^{3/4} - 0.43393\lambda^{1/4} + \dots, \\ g''(0) &\sim 0.496728\lambda^{1/4} + 2.59746\lambda^{-1/4} + \dots, \\ \theta'(0) &\sim -0.752735\lambda^{1/4} + 0.160829\lambda^{-1/4} + \dots,\end{aligned}$$

for $Pr = 1$ and $\gamma = 0.6$, when $M = 4.5$,

$$\begin{aligned}\phi_0''(0) &= 0.935402, & h_0''(0) &= 0.496728, & \theta_0'(0) &= -0.752735, \\ \phi_1''(0) &= -0.771636, & h_1''(0) &= 4.19369, & \theta_1'(0) &= 0.339145, \\ f''(0) &\sim 0.935402\lambda^{3/4} - 0.771636\lambda^{1/4} + \dots, \\ g''(0) &\sim 0.496728\lambda^{1/4} + 4.19369\lambda^{-1/4} + \dots, \\ \theta'(0) &\sim -0.752735\lambda^{1/4} + 0.339145\lambda^{-1/4} + \dots\end{aligned}$$

as $\lambda \rightarrow \infty$.

3 Stability analysis

Numerically, it is seen that there are two branches of solution for distinct values of the physical parameter. Here we have performed a stability analysis of the boundary value problem to identify whether the dual solutions are stable or unstable. A number of researchers performed stability analyses to identify the stable solution, including Merkin [20], Weidman et al. [30], Harris et al. [9], Mahapatra and Nandy [15], Rosca and Pop [25]. They all noted that the upper branch solution is stable, while the lower branch solution is unstable. We explore the unsteady similarity solution in the form

$$\begin{aligned}u &= (a + b)x \frac{\partial f}{\partial \eta}(\eta, \tau), & v &= (a - b)y \frac{\partial g}{\partial \eta}(\eta, \tau), \\ w &= -\sqrt{\frac{\nu}{a}} [(a + b)f(\eta, \tau) + (a - b)g(\eta, \tau)], \\ T - T_\infty &= T_0 x \theta(\eta, \tau), & \eta &= \sqrt{\frac{a}{\nu}} z, & \tau &= (a + b)t,\end{aligned}$$

where τ is a newly introduced nondimensional time variable. Thus, Eqs. (8)–(10) can be expressed as

$$\begin{aligned} \frac{\partial^3 f}{\partial \eta^3} + (1 + \gamma) \left[f \frac{\partial^2 f}{\partial \eta^2} + 1 - \left(\frac{\partial f}{\partial \eta} \right)^2 \right] + (1 - \gamma) g \frac{\partial^2 f}{\partial \eta^2} \\ + (1 + \gamma) \lambda \theta + M \left(1 - \frac{\partial f}{\partial \eta} \right) - (1 + \gamma) \frac{\partial^2 f}{\partial \eta \partial \tau} = 0, \end{aligned} \tag{25}$$

$$\begin{aligned} \frac{\partial^3 g}{\partial \eta^3} + (1 - \gamma) \left[g \frac{\partial^2 g}{\partial \eta^2} + 1 - \left(\frac{\partial g}{\partial \eta} \right)^2 \right] + (1 + \gamma) f \frac{\partial^2 g}{\partial \eta^2} \\ + M \left(1 - \frac{\partial g}{\partial \eta} \right) - (1 + \gamma) \frac{\partial^2 g}{\partial \eta \partial \tau} = 0, \end{aligned} \tag{26}$$

$$\frac{1}{Pr} \frac{\partial^2 \theta}{\partial \eta^2} + (1 + \gamma) \left(f \frac{\partial \theta}{\partial \eta} - \frac{\partial f}{\partial \eta} \theta \right) + (1 - \gamma) g \frac{\partial \theta}{\partial \eta} - (1 + \gamma) \frac{\partial \theta}{\partial \tau} = 0 \tag{27}$$

with the corresponding boundary conditions

$$\begin{aligned} f(0, \tau) = \frac{\partial f}{\partial \eta}(0, \tau) = 0, \quad g(0, \tau) = \frac{\partial g}{\partial \eta}(0, \tau) = 0, \quad \theta(0, \tau) = 1, \\ \frac{\partial f}{\partial \eta}(\eta, \tau) \rightarrow 1, \quad \frac{\partial g}{\partial \eta}(\eta, \tau) \rightarrow 1, \quad \theta(\eta, \tau) \rightarrow 0 \quad \text{as } \eta \rightarrow \infty. \end{aligned} \tag{28}$$

The stability analysis of the steady flow solution was examined by setting $f(\eta) = f_0(\eta)$, $g(\eta) = g_0(\eta)$, and $\theta(\eta) = \theta_0(\eta)$ satisfying the boundary value problem (8)–(11). According to Merkin [20] and Harris et al. [9], we can write

$$\begin{aligned} f(\eta, \tau) &= f_0(\eta) + e^{-\epsilon \tau} F(\eta, \tau), \\ g(\eta, \tau) &= g_0(\eta) + e^{-\epsilon \tau} G(\eta, \tau), \\ \theta(\eta, \tau) &= \theta_0(\eta) + e^{-\epsilon \tau} H(\eta, \tau), \end{aligned} \tag{29}$$

where ϵ is an unknown eigenvalue that represents the growth rate of the disturbance. Here $F(\eta, \tau)$, $G(\eta, \tau)$, and $H(\eta, \tau)$ are small relative to $f_0(\eta)$, $g_0(\eta)$, and $\theta_0(\eta)$. As recommended by Weidman et al. [30], we examine the stability of the steady flow and heat transfer solutions $f_0(\eta)$, $g_0(\eta)$, and $\theta_0(\eta)$ by setting $\tau = 0$. Thus, $F(\eta, 0) = F_0(\eta)$, $G(\eta, 0) = G_0(\eta)$, and $H(\eta, 0) = H_0(\eta)$ in Eqs. (25)–(28) respectively indicate the initial growth or decay of the solution (29). We obtain the following linear eigenvalue problem:

$$\begin{aligned} F_0''' + (1 + \gamma)(f_0 F_0'' + f_0'' F_0 - 2f_0' F_0' + \lambda H_0 + \epsilon F_0') \\ + (1 - \gamma)(g_0 F_0'' + G_0 f_0'') - M F_0' = 0, \end{aligned} \tag{30}$$

$$\begin{aligned} G_0''' + (1 - \gamma)(g_0 G_0'' + G_0 g_0'' - 2g_0' G_0') + (1 + \gamma)(f_0 G_0'' + F_0 g_0'') \\ - M G_0' + (1 + \gamma)\epsilon G_0' = 0, \end{aligned} \tag{31}$$

$$\begin{aligned} \frac{1}{Pr} H_0'' + (1 + \gamma)(f_0 H_0' + F_0 \theta_0' - f_0' H_0 - F_0' \theta_0 + \epsilon H_0) \\ + (1 - \gamma)(g_0 H_0' + G_0 \theta_0') = 0 \end{aligned} \tag{32}$$

with the boundary conditions

$$\begin{aligned} F_0(0) = F'_0(0) = 0, \quad G_0(0) = G'_0(0) = 0, \quad H_0(0) = 0, \\ F'_0(\eta) \rightarrow 0, \quad G'_0(\eta) \rightarrow 0, \quad H_0(\eta) \rightarrow 0 \quad \text{as } \eta \rightarrow \infty. \end{aligned} \quad (33)$$

It should be noted that for particular values of λ , γ , M , and Pr , the stability of the related steady flow solutions $f_0(\eta)$, $g_0(\eta)$, and $\theta_0(\eta)$ are determined by the smallest eigenvalue ϵ . According to Harris et al. [9], we can determine the range of possible eigenvalues by relaxing a boundary condition on $F_0(\eta)$, $G_0(\eta)$, or $H_0(\eta)$. We relax the condition $F'_0(\eta) \rightarrow 0$ as $\eta \rightarrow \infty$ for the current problem. Consequently, for a fixed value of ϵ , we solve the system of Eqs. (30)–(33) along with the newly introduced boundary condition $F''_0(0) = 1$.

4 Numerical solution procedure

The governing momentum equations are solved numerically using the fourth-order Runge–Kutta method with the shooting technique in Mathematica. The equations are written as a system of eight first-order ordinary differential equations, which are solved using a standard fourth-order Runge–Kutta integration method. Then, for convergence, a Newton iteration method is used. The system of nonlinear ordinary differential equations (8)–(10) along with the boundary conditions (11) are solved numerically using shooting technique by converting it to an initial value problem. To do this, we need first to rewrite the system of nonlinear ordinary differential equations (8)–(10) as a system of eight first-order ordinary differential equations as

$$\begin{aligned} y'_1 &= y_2, & y'_2 &= y_3, \\ y'_3 &= -(1 + \gamma)(y_1 y_3 + 1 - y_2^2) - (1 - \gamma)y_4 y_3 - (1 + \gamma)\lambda y_7 - M(1 - y_2), \\ y'_4 &= y_5, & y'_5 &= y_6, \\ y'_6 &= -(1 - \gamma)(y_4 y_6 + 1 - y_5^2) - (1 + \gamma)y_1 y_6 - M(1 - y_5), \\ y'_7 &= y_8, & y'_8 &= -Pr(1 + \gamma)(y_1 y_8 - y_2 y_7) - Pr(1 - \gamma)y_4 y_8. \end{aligned}$$

The corresponding boundary conditions (11) become

$$\begin{aligned} y_1(0) = 0, & \quad y_2(0) = 0, & \quad y_3(0) = W_1, & \quad y_4(0) = 0, \\ y_5(0) = 0, & \quad y_6(0) = W_2, & \quad y_7(0) = 1, & \quad y_8(0) = W_3, \end{aligned}$$

where $y_1 = f$, $y_2 = f'$, $y_3 = f''$, $y_4 = g$, $y_5 = g'$, $y_6 = g''$, $y_7 = \theta$, $y_8 = \theta'$, and the values of W_1 , W_2 , and W_3 are determined such that they satisfy the outer boundary conditions $y_2(\infty)$, $y_5(\infty)$, and $y_7(\infty)$. We integrate the resulting first-order differential equations by using a fourth-order Runge–Kutta method. Then the shooting method is employed to predict the values of W_1 , W_2 , and W_3 by iterations until the outer boundary conditions are satisfied. To this end, we adjust the values of W_1 , W_2 , and W_3 at $\eta = 0$ by using a Newton iteration method to assure quadratic convergence of the iterations.

We repeated the above procedure until we get the results up to the appropriate degree of accuracy, 10^{-5} . For this numerical method, $\eta_\infty = 8$ has been chosen for searching the possible steady flow solutions (upper and lower branch solutions) with the various values of the governing parameters considered in this problem.

5 Results and discussion

The system of nonlinear ordinary differential equations (8)–(11) has been solved numerically for some values of the mixed convection parameter λ , magnetic field parameter M , and shear-to-strain-rate ratio γ , while the Prandtl number Pr is set to be unity ($Pr = 1$).

By comparing the numerical results with previous studies it was discovered that there was considerable agreement, which are shown in Table 1, and thus we are assured that the current approach is accurate. The outcomes demonstrate the impact of some significant nondimensional parameters on the features of flow and temperature characteristics. Representative skin friction coefficients $f''(0)$, $g''(0)$, surface temperature gradient $\theta'(0)$, velocity and temperature profiles are shown in Figs. 1–3. Figures 1(a), 1(c), 1(e) show the variation of skin friction coefficients $f''(0)$, $g''(0)$ and surface temperature gradient $\theta'(0)$ with shear-to strain-rate ratio γ over the range $-4 \leq \gamma \leq 4$ for $\lambda = 0$ (forced convection) and some values of magnetic field parameter M . From Figs. 1(a), 1(c) it is observed that $f''(0)$ and $g''(0)$ increase with the γ as the magnetic field parameter M increases. Figure 1(e) also shows that $\theta'(0)$ increases with the increase in magnetic field parameter M for a particular value of γ when $-4 \leq \gamma \leq -1.3$, but the opposite trend is observed for a specific value of γ when $\gamma > -1.3$. The variations of the skin friction coefficients $f''(0)$, $g''(0)$ and surface temperature gradient $\theta'(0)$ with mixed convection parameter λ for magnetic field parameter M are shown in Figs. 1(b), 1(d), 1(f) and 2(a), 2(c), 2(e), all for $Pr = 1$. From Figs. 1(b), 1(d), 1(f) it is found that the skin friction coefficients $f''(0)$ and $g''(0)$ increase as the magnetic field parameter M increases. This observation is due to the fact that the effect of magnetic field reduces the boundary layer thickness, which, in turn, increases the skin friction. In Figs. 1(b), 1(d), 1(f), it is observed that $f''(0)$ (upper and lower branch solution) and $g''(0)$ (upper and lower branch solution) increase with the increase of λ for a particular value of γ and M , while $\theta'(0)$ (upper branch solution) decreases. Figures 2(a), 2(c), 2(e) show the variations of the skin friction coefficients $f''(0)$, $g''(0)$ and surface temperature gradient $\theta'(0)$ with mixed convection parameter λ for $M = 0, 0.4, 0.8$ when $\gamma = 0.5$. From Figs. 2(a), 2(c), 2(e) it is noticed that the enhancement of the magnetic field parameter M leads to increase the

Table 1. Comparison of $f''(0)$ and $g''(0)$ for different values of λ when $\gamma = 0$, $M = 0$, and $Pr = 1$.

λ	Present result		Lok et al. [13]	
	$f''(0)$	$g''(0)$	$f''(0)$	$g''(0)$
0.5	1.51148	1.31847	1.50195	1.31250
1.0	1.70503	1.32466	1.70313	1.32656
1.5	1.89337	1.33054	1.89063	1.33125
2.0	2.07712	1.33616	2.06251	1.33807

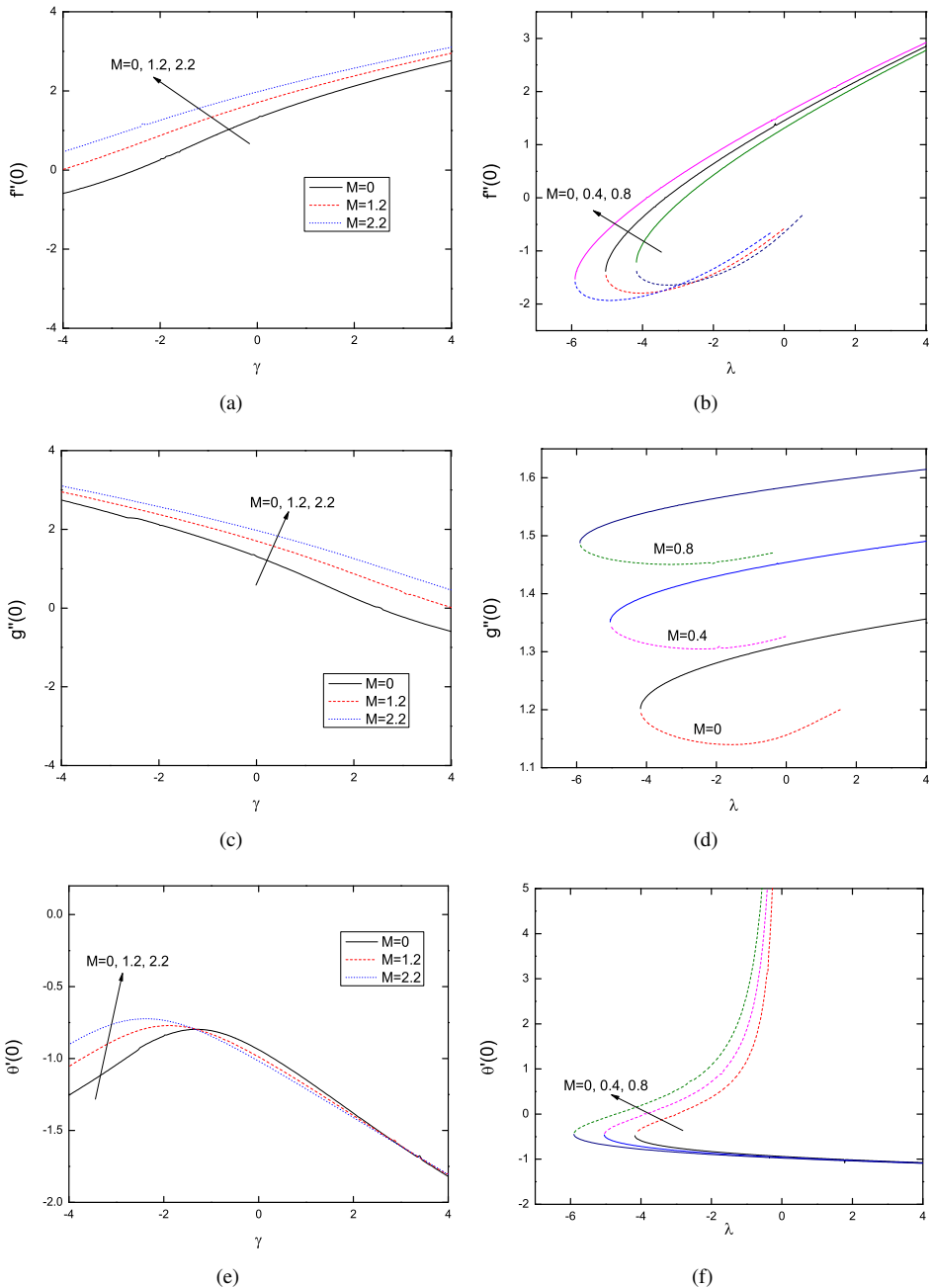


Figure 1. Plots of $f''(0)$, $g''(0)$, and $\theta'(0)$: (a), (c), (e) against γ for $M = 0, 1.2, 2.2$ and $\lambda = 0$ obtained from the numerical solution of (8)–(11) ($Pr = 1$); (b), (d), (f) against λ for $M = 0, 0.4, 0.8$ and $\gamma = 0$ obtained from the numerical solution of (8)–(11) ($Pr = 1$).

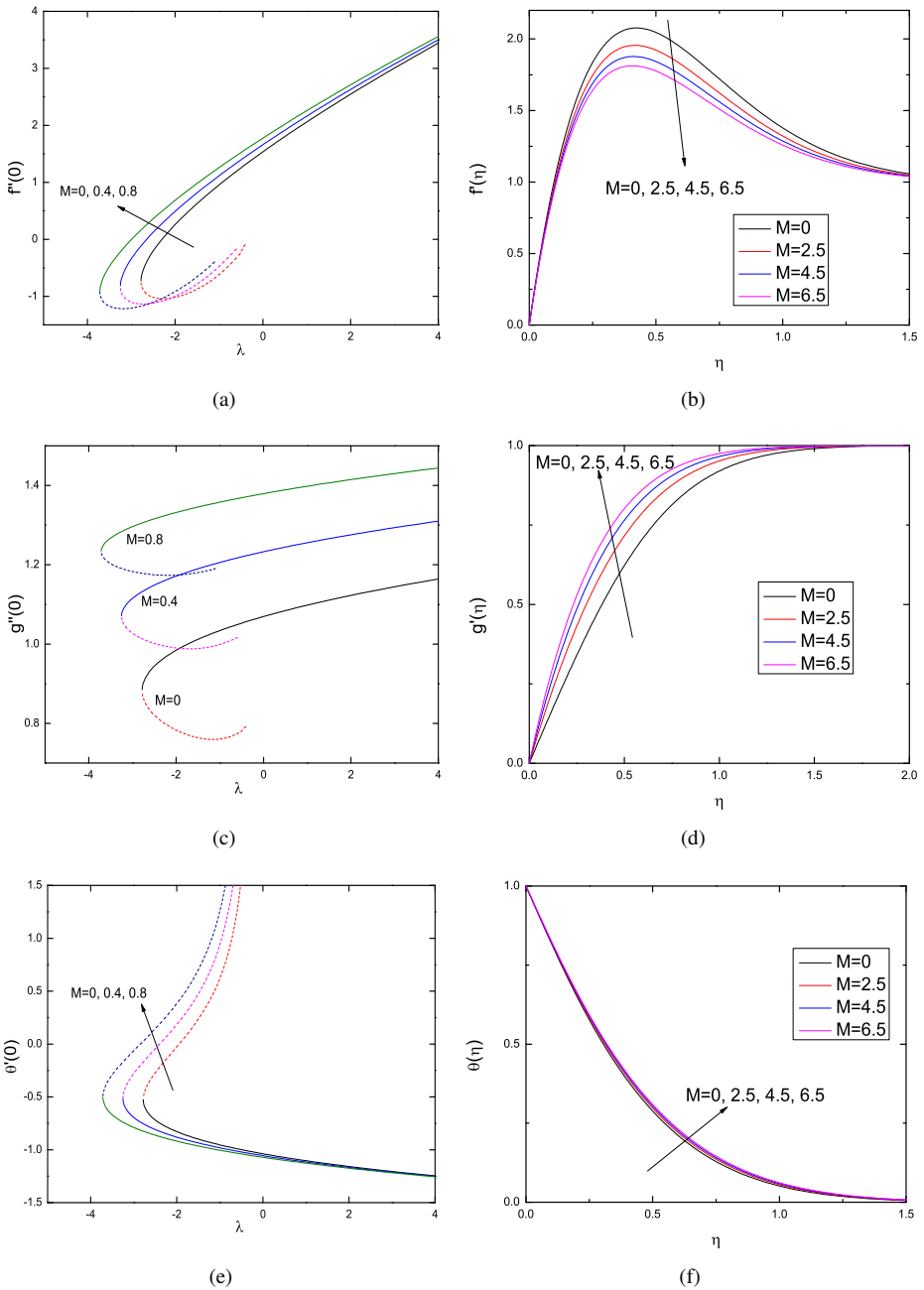


Figure 2. (a), (c), (e) Plots of $f''(0)$, $g''(0)$, and $\theta'(0)$ against λ for $M = 0, 0.4, 0.8$ and $\gamma = 0.5$ obtained from the numerical solution of (8)–(11) ($Pr = 1$). (b), (d), (f) Velocity profiles $f'(\eta)$, $g'(\eta)$ and temperature profile $\theta(\eta)$ for various values of $M = 0, 2.5, 4.5, 6.5$ when $\lambda = 30$ (large λ), $\gamma = 0.6$, and $Pr = 1$.

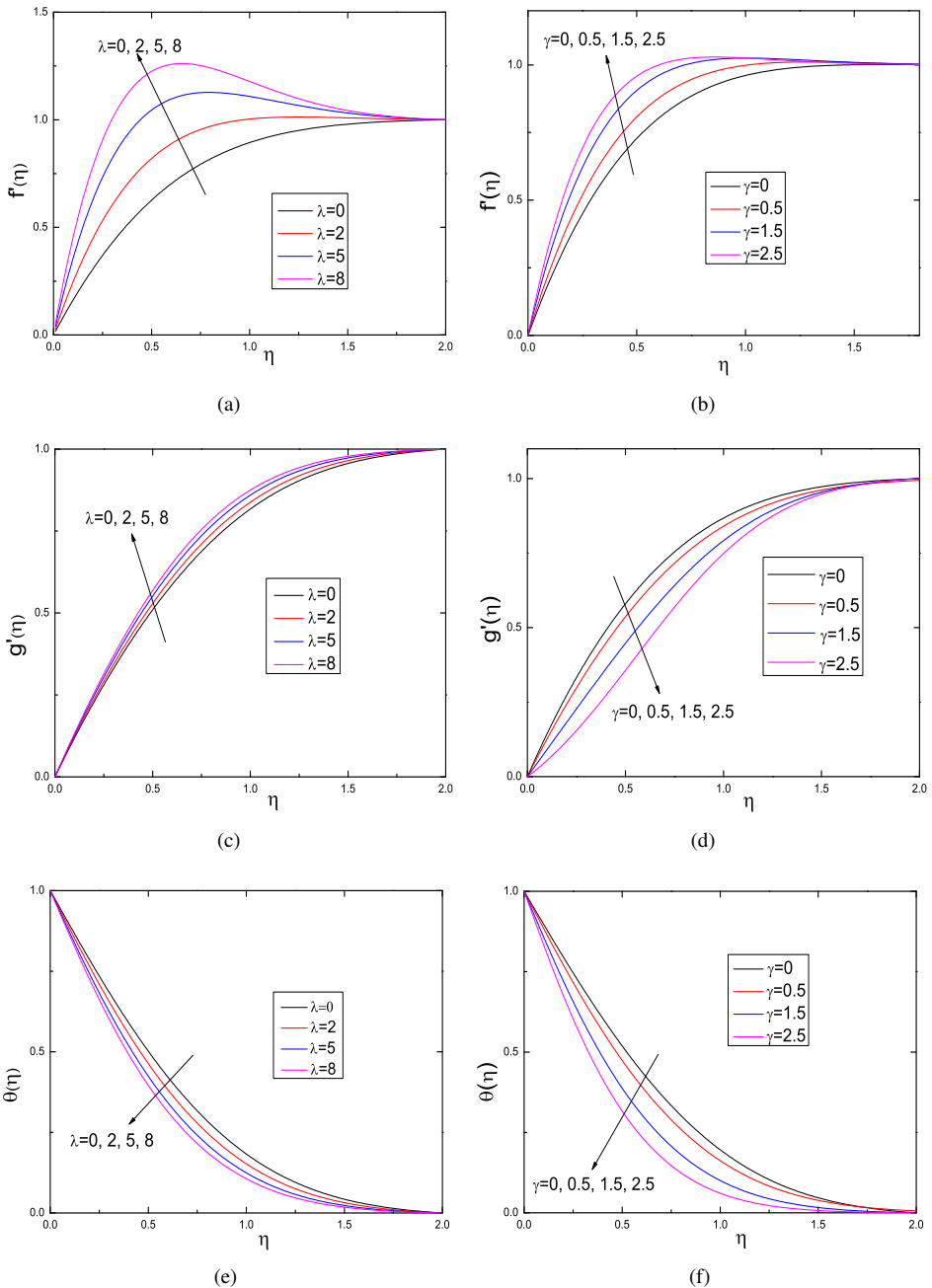


Figure 3. Velocity profiles $f'(\eta)$, $g'(\eta)$ and temperature profile $\theta(\eta)$: (a), (c), (e) for various values of $\lambda = 0, 2, 5, 8$ when $M = 0.5$, $\gamma = 0.6$, and $Pr = 1$; (b), (d), (f) for various values of $\gamma = 0, 0.5, 1.5, 2.5$ when $M = 0.5$, $\lambda = 2$, and $Pr = 1$.

Table 2. Smallest eigenvalue ϵ_1 for several values of λ with $\gamma = 0.5$, $M = 0.4$, and $Pr = 1$.

λ	Upper branch solution ϵ_1	Lower branch solution ϵ_1
-0.8	3.2501	-1.53346
-1.2	2.73275	-1.37096
-1.6	2.59371	-1.18125
-2.0	2.3101	-0.95954

skin friction coefficients. Here solid lines represent the upper branch solution, and dashed lines represent the corresponding lower branch solution. These figures illustrate that it is possible to find dual solution of the similarity equations (8)–(11). For negative values of λ , there is a critical value $\lambda_c (< 0)$ with two solutions branches for $\lambda > \lambda_c$, a saddle-node bifurcation at $\lambda = \lambda_c$, and for $\lambda < \lambda_c$, there is no solution.

In comparison to the lower branch solutions, the upper branch solutions have higher value of $f''(0)$, $g''(0)$, and $\theta'(0)$ for a particular value of λ . These figures also demonstrate that as the magnetic field parameter M increases, the critical value $|\lambda_c|$ increases.

Representative results for the velocity and temperature profiles are displayed in Figs. 2(b), 2(d), 2(f), and 3(a)–3(f). Figures 2(b), 2(d), 2(f) show the variation in velocity profiles $f'(\eta)$, $g'(\eta)$, and temperature profile $\theta(\eta)$ with η for several values of the magnetic field parameter M . The effect of the magnetic field on velocity and temperature profiles is shown in Figs. 2(b), 2(d), 2(f). From Fig. 2(b) we observe that as the magnetic field parameter M increases, velocity along the x -axis decreases. Figure 2(d) shows that as the magnetic field parameter M increases, velocity along the y -axis increases. It is clear from Fig. 2(f) that temperature at a point increases with the increase of the magnetic field parameter M . The reason is that when a system's magnetic field rises, resistance forces are created against the flow, which will cause a reduction in the velocity field. However, making friction between the magnetic field and the electric field within the flow-stream layer, enhances the temperature profile. In Figs. 3(a), 3(c), 3(e), velocity and temperature profiles are shown for different values of mixed convection parameter λ . It is seen from Figs. 3(a) and 3(c) that the velocities $f'(\eta)$ and $g'(\eta)$ increase with the increase of λ . Figure 3(e) shows that the temperature $\theta(\eta)$ decreases with the rise of λ . Figures 3(b), 3(d), 3(f) show the effect of γ on velocity and temperature profiles. From Figs. 3(b), 3(d), and 3(f) it is noticed that when the value of the shear-to strain-rate ratio γ increases, the velocity along the x -axis increases, while along the y -axis it decreases. It is also observed that temperature at a point decreases when γ increases. A stability analysis has been performed by solving the eigenvalue problem generated by Eqs. (30)–(32) subject to the boundary conditions (33) and determining which of the solutions is stable. Solutions of the eigenvalue problem (30)–(33) give an infinite set of eigenvalues $\epsilon_1 < \epsilon_2 < \epsilon_3 < \dots$. When the smallest eigenvalue ϵ_1 is negative, the flow becomes unstable, and there is an initial growth of disturbances. Conversely, if ϵ_1 is positive, the flow becomes stable, and there is an early decline of disturbances. The smallest eigenvalues ϵ_1 for different values of the mixed convection parameter λ are displayed in Table 2.

From this table it is observed that the upper branch solutions contain positive eigenvalues ϵ_1 , while the lower branch solutions contain negative eigenvalues ϵ_1 . As a result,

we obtain the conclusion that the first (upper branch) solution is stable, while the second (lower branch) solution is unstable. The basic fluid flow problem, which is considered here, was investigated by Weidman [29], and the corresponding mixed convection flow was studied by Lok et al. [13]. When a constant magnetic field is applied in the normal direction to the buoyancy force, the Lorentz force is generated due to the fluid velocity. This Lorentz force has a significant influence on the mixed convection, which is evident from different figures presented here.

6 Concluding remarks

We have considered the steady mixed convection nonaxisymmetric Homann stagnation-point flow of an incompressible viscous fluid over a vertical flat wall in a magnetic field. The governing equations are transformed into ordinary differential equations by applying similarity transformations. The equations for the flow and temperature fields reduce to similarity form and involve four parameters: the Prandtl number Pr , γ representing the shear-to-strain-rate ratio, magnetic field parameter M , and a mixed convection parameter λ . The transformed equations are solved numerically by an efficient shooting method. The characteristics of the skin friction coefficient, surface temperature gradient, velocity, and temperature features for governing parameters are analyzed and discussed. We have shown how the solutions behave for all λ for representative values of magnetic field parameter M . The enhancement of the magnetic field parameter M leads to increase the skin friction coefficient. It is observed that when the mixed convection parameter λ is large, the upper branch values of $f''(0)$ and $g''(0)$ increase at a constant rate. It is noticed that as the magnetic field parameter M increases, the critical value $|\lambda_c|$ increases. Also, it is found that dual solutions exist for a specific range of mixed convection parameter λ . From the stability analysis it is concluded that the upper branch solutions are stable and physically realizable, while the lower branch solutions are unstable. When the magnetic field parameter M increases, the fluid velocity along the x -axis decreases, whereas along the y -axis fluid velocity increases. With the increases of mixed convection parameter λ , the fluid velocity increases. It is noticed that when the shear-to strain-rate ratio γ increases, the velocity profile increases along the x -axis but decreases along the y -axis. Also, we observe that when the shear-to-strain-rate ratio γ increases, the temperature at a point decreases.

Acknowledgment. The authors wish to express their very sincere thanks to the reviewers for their very good comments and suggestions. One of the authors, C.M. Mardi, is grateful to the Council of Scientific and Industrial Research (CSIR), New Delhi, India, for providing financial support for the realization of this work.

References

1. P.D. Ariel, Hiemenz flow in hydromagnetics, *Acta Mech.*, **103**(1):31–43, 1994, <https://doi.org/10.1007/BF01180216>.

2. A. Bejan, *Convection Heat Transfer*, John Wiley & Sons, Hoboken, NJ, 2013.
3. T.S. Chen, Mixed convection in external flow, in *Handbook of Single-Phase Convective Heat Transfer*, John Wiley & Sons, New York, 1987, pp. 14.1–14.35, <https://cir.nii.ac.jp/crid/1574231874542445568>.
4. E.R.G. Eckert, Die Berechnung des Wärmeüberganges in der laminaren Grenzschicht umstromter Körper, *VDI Forschungsheft*, **416**:1–24, 1942, <https://cir.nii.ac.jp/crid/1571980075311159424>.
5. N.T. Eldabe, Mahmoud E.M. Ouaf, Chebyshev finite difference method for heat and mass transfer in a hydromagnetic flow of a micropolar fluid past a stretching surface with Ohmic heating and viscous dissipation, *Appl. Math. Comput.*, **177**(2):561–571, 2006, <https://doi.org/10.1016/j.amc.2005.07.071>.
6. B. Gebhart, Y. Jaluria, R.L. Mahajan, B. Sammakia, *Buoyancy-Induced Flows and Transport*, CRC Press, New York, 1988.
7. R.S.R. Gorla, Heat transfer in an axisymmetric stagnation flow on a cylinder, *Appl. Sci. Res.*, **32**:541–553, 1976, <https://doi.org/10.1007/BF00385923>.
8. A.G. Hansen, *Similarity Analyses of Boundary Value Problems in Engineering*, Englewood Cliffs, NJ, 1964, <https://cir.nii.ac.jp/crid/1130282273159410304>.
9. S.D. Harris, D.B. Ingham, I. Pop, Mixed convection boundary-layer flow near the stagnation point on a vertical surface in a porous medium: Brinkman model with slip, *Transp. Porous Med.*, **77**:267–285, 2009, <https://doi.org/10.1007/s11242-008-9309-6>.
10. K. Hiemenz, Die Grenzschicht an einem in den gleichförmigen Flüssigkeitsstrom eingetauchten geraden Kreiszyylinder, *Dinglers Polytech. J.*, **326**:321–324, 1911, <https://cir.nii.ac.jp/crid/1573668924607721856>.
11. F. Homann, Der Einfluss grosser Zähigkeit bei der Strömung um den Zylinder und um die Kugel, *Z. Angew. Math. Mech.*, **16**(3):153–164, 1936, <https://doi.org/10.1002/zamm.19360160304>.
12. A. Ishak, R. Nazar, I. Pop, Magnetohydrodynamic (MHD) flow of a micropolar fluid towards a stagnation point on a vertical surface, *Comput. Math. Appl.*, **56**(12):3188–3194, 2008, <https://doi.org/10.1016/j.camwa.2008.09.013>.
13. Y.Y. Lok, J.H. Merkin, I. Pop, Mixed convection non-axisymmetric Homann stagnation-point flow, *J. Fluid Mech.*, **812**:418–434, 2017, <https://doi.org/10.1017/jfm.2016.809>.
14. T.R. Mahapatra, A.S. Gupta, Magnetohydrodynamic stagnation-point flow towards a stretching sheet, *Acta Mech.*, **152**(1):191–196, 2001, <https://doi.org/10.1007/BF01176953>.
15. T.R. Mahapatra, S.K. Nandy, Stability analysis of dual solutions in stagnation-point flow and heat transfer over a power-law shrinking surface, *Int. J. Nonlinear Sci.*, **12**(1):86–94, 2011.
16. T.R. Mahapatra, S. Sidui, Unsteady heat transfer in non-axisymmetric Homann stagnation-point flows, *Z. Angew. Math. Phys.*, **68**(2):32, 2017, <https://doi.org/10.1007/s00033-017-0775-y>.
17. T.R. Mahapatra, S. Sidui, Non-axisymmetric homann stagnation-point flow of a viscoelastic fluid towards a fixed plate, *Eur. J. Mech., B, Fluids*, **79**:38–43, 2020, <https://doi.org/10.1016/j.euromechflu.2019.08.010>.

18. T. Mahmood, J.H. Merkin, Mixed convection on a vertical circular cylinder, *Z. Angew. Math. Phys.*, **39**(2):186–203, 1988, <https://doi.org/10.1007/BF00945765>.
19. T. Mahmood, J.H. Merkin, Similarity solutions in axisymmetric mixed-convection boundary-layer flow, *J. Eng. Math.*, **22**:73–92, 1988, <https://doi.org/10.1007/BF00044366>.
20. J.H. Merkin, Mixed convection boundary layer flow on a vertical surface in a saturated porous medium, *J. Eng. Math.*, **14**(4):301–313, 1980, <https://doi.org/10.1007/BF00052913>.
21. J.H. Merkin, T. Mahmood, Mixed convection boundary layer similarity solutions: Prescribed wall heat flux, *Z. Angew. Math. Phys.*, **40**(1):51–68, 1989, <https://doi.org/10.1007/BF00945309>.
22. J.H. Merkin, I. Pop, Mixed convection along a vertical surface: Similarity solutions for uniform flow, *Fluid Dyn. Res.*, **30**(4):233, 2002, [https://doi.org/10.1016/S0169-5983\(02\)00042-4](https://doi.org/10.1016/S0169-5983(02)00042-4).
23. I. Pop, D.B. Ingham, *Convective Heat Transfer: Mathematical and Computational Modelling of Viscous Fluids and Porous Media*, Elsevier, Amsterdam, 2001.
24. N. Ramachandran, T.S. Chen, B.F. Armaly, Mixed convection in stagnation flows adjacent to vertical surfaces, *J. Heat Transfer*, **110**(2):373–377, 1988, <https://doi.org/10.1115/1.3250494>.
25. A.V. Roşca, I. Pop, Flow and heat transfer over a vertical permeable stretching/shrinking sheet with a second order slip, *Int. J. Heat Mass Transfer*, **60**:355–364, 2013, <https://doi.org/10.1016/j.ijheatmasstransfer.2012.12.028>.
26. H. Schlichting, K. Gersten, *Boundary-Layer Theory*, Springer, Berlin, Heidelberg, 2016, <https://doi.org/10.1007/978-3-662-52919-5>.
27. F.T. Smith, Three dimensional stagnation point flow into a corner, *Proc. R. Soc. Lond., A, Math. Phys. Eng. Sci.*, **344**(1639):489–507, 1975, <https://doi.org/10.1098/rspa.1975.0116>.
28. C.Y. Wang, Axisymmetric stagnation flow on a cylinder, *Q. Appl. Math.*, **32**(2):207–213, 1974, <https://doi.org/10.1090/qam/99683>.
29. P.D. Weidman, Non-axisymmetric Homann stagnation-point flows, *J. Fluid Mech.*, **702**:460–469, 2012, <https://doi.org/10.1017/jfm.2012.197>.
30. P.D. Weidman, D.G. Kubitschek, A.M.J. Davis, The effect of transpiration on self-similar boundary layer flow over moving surfaces, *Int. J. Eng. Sci.*, **44**(11–12):730–737, 2006, <https://doi.org/10.1016/j.ijengsci.2006.04.005>.